Materials Research. 2026; 29(Suppl. 2): e20260131
DOI: https://doi.org/10.1590/1980-5373-MR-2026-0131

Graphene Oxide/Polydopamine (GO/PDA) Coated Membranes for Selective Filtration of Cationic and Anionic Dyes

***Bianca Lorraine Rodrigues dos Santos*[a], *Bruna Oliveira Salla do Carmo*[a], *Celina Massumi Miyazaki*[a], *Guilherme Dognani*[a]* , *Priscila Alessio*[a]**

[a]*Universidade Estadual Paulista (UNESP), Faculdade de Ciências e Tecnologia, Presidente Prudente, SP, Brasil*

Received: April 26, 2026; Revised: June 10, 2026; Accepted: July 09, 2026

The discharge of synthetic dyes into industrial effluents represents a major environmental challenge due to their high stability and persistence in aquatic systems. Among available treatment strategies, membrane-based separation processes have emerged as promising alternatives for removing organic contaminants from water. However, improving membrane selectivity and efficiency toward different classes of dyes remains an important challenge. In this study, commercial PVDF membranes were modified with polydopamine (PDA) and a graphene oxide/polydopamine (GO/PDA) composite to evaluate their performance in removing methylene blue (MB, a cationic dye) and Congo red (CR, an anionic dye). The modified membranes were prepared through surface deposition of active layers and characterized using UV–Vis spectroscopy, FTIR spectroscopy, scanning electron microscopy (SEM), atomic force microscopy (AFM), and water contact angle (WCA) measurements. Filtration experiments were carried out to assess dye removal efficiency and selectivity. The results showed that PDA-modified membranes achieved the highest retention efficiency for MB and the mixture, indicating a significant improvement over the unmodified PVDF membrane. However, the pristine membrane exhibited a higher retention of the anionic dye. The incorporation of GO contributed to a more homogeneous surface and enhanced selective filtration behavior. In mixed dye solutions (1:1 MB: CR), the GO/PDA membrane demonstrated a greater ability to preferentially remove CR, with a selectivity factor of 3.50. Overall, the deposition of PDA-based layers proved a promising strategy for enhancing nanofiltration membrane performance in the treatment of dye-containing effluents, while GO/PDA modification improved membrane selectivity.

Keywords: *Membrane filtration, membrane modification, dye retention, graphene oxide composite, selective filtration.*

1. Introduction

The growth of industrialization worldwide has created several societal challenges, particularly environmental issues. Industries such as textiles are known to be among the main contributors to environmental problems[1]. Projections show that the global textile market was estimated at USD 1.11 trillion in 2024 and is projected to reach USD 1.61 trillion by 2033[2]. To reduce its impact on environmental pollution, particularly water contamination, this industry has sought to adopt cleaner production processes[3,4].

However, conventional systems operated by most textile industries have led to the uncontrolled release of synthetic dyes into aquatic environments, emerging as a critical environmental challenge due to their chemical stability, resistance to degradation, and long-term persistence in water bodies[5,6]. These characteristics not only compromise water quality but also pose risks to aquatic ecosystems and human health, underscoring the urgent need for efficient and selective wastewater treatment technologies[5,7]. In this context, membrane-based processes have attracted considerable attention owing to their operational simplicity, scalability, and high separation efficiency[8,9].

Membrane technologies encompass a wide range of separation processes that differ mainly in their pore size and operating pressure, including microfiltration (MF), ultrafiltration (UF), nanofiltration (NF), and reverse osmosis (RO). Among these, NF has attracted particular interest for the treatment of dye-contaminated wastewater due to its ability to retain multivalent ions and organic molecules while operating at relatively moderate pressures[10]. NF membranes typically possess pore sizes in the nanometer range and exhibit separation mechanisms driven by a combination of steric hindrance, electrostatic interactions, and adsorption[11,12]. As a result, these membranes can effectively remove a wide variety of organic dyes, salts, and other emerging contaminants from aqueous solutions. Nevertheless, conventional polymeric membranes may still face limitations such as limited selectivity toward molecules of similar size, restricted surface functionality, and membrane fouling, which can compromise their long-term performance in complex effluents[11,13,14].

*e-mail: *guilherme.dognani@unesp.br*
Associate Editor: Luis Cabral.
Editor-in-Chief: Luiz Antonio Pessan.

To overcome these limitations, several strategies have been explored to modify membrane surfaces and improve their properties. Surface modification can enhance hydrophilicity, control surface charge, increase permeability, and introduce selective interactions between the membrane and target pollutants[15,16]. Among the different approaches reported in the literature, coating or functionalization with bioinspired polymers[17,18], nanomaterials[19,20], or hybrid composites[21,22] have shown particularly promising results. Polydopamine (PDA), inspired by the adhesive proteins of mussels, has gained significant attention due to its strong adhesion to a wide variety of substrates and its ability to introduce reactive functional groups onto membrane surfaces[18,23,24]. In addition, the incorporation of nanomaterials such as graphene oxide (GO) can further improve membrane performance by increasing surface area, tuning surface charge, and promoting selective transport pathways[19,25].

Building upon these advances, the present study evaluates PVDF membranes coated with PDA and GO/PDA, with particular emphasis on their ability to achieve selective nanofiltration of cationic and anionic dyes. The influence of surface modification on membrane properties, adsorption behavior, and separation performance was investigated, highlighting the potential of the GO/PDA layer as a rational strategy for tuning membrane selectivity in the treatment of dye-contaminated wastewater. The synergistic combination of PDA and GO has therefore emerged as an attractive strategy for fabricating membranes with improved stability, enhanced antifouling behavior, and greater selectivity toward specific contaminants.

2. Experimental

2.1. Materials

Commercial polyvinylidene fluoride (PVDF) membranes with 0.22 µm pore size (Millipore, USA) were used as substrates for deposition of the active layer. The reagents used for PDA polymerization and membrane modification were dopamine hydrochloride (Sigma-Aldrich, purity ≥ 98%), tris(hydroxymethyl)aminomethane (TRIS, Sigma-Aldrich, ACS reagent, purity 99.8%), sodium hydroxide (NaOH, F. Maia Indústria e Comércio Ltda, purity ≥ 97%), and graphene oxide (GO, Sigma-Aldrich, aqueous dispersion of 2 mg mL^{-1}). The dyes employed were methylene blue (MB, Synth®, cationic dye, purity ≥ 82%) and Congo red (CR, Synth®, anionic dye). All solutions were prepared using ultrapure water from the Milli-Q system (18.2 MΩ·cm).

2.2. Synthesis and polymerization of dopamine

For dopamine polymerization, 0.05 g of dopamine was added to a 10 mL aqueous TRIS solution at 5 mg mL^{-1}, and the pH was adjusted to 8.5 using NaOH solutions (0.5 and 0.1 mol L^{-1}). The reaction mixture was stirred continuously at 80 °C for 24 h to promote the formation of dark brown polydopamine (PDA). After polymerization, the solution was diluted and sonicated to achieve complete homogenization, then deposited onto the membrane surface.

2.3. Preparation of the GO/PDA suspension

First, 4 mL of the GO aqueous dispersion (1 mL of commercial 2 mg mL^{-1} dispersion + 3 mL of ultrapure water kept under sonication for 30 min) were diluted once more with ultrapure water to a final volume of 25 mL and sonicated for an additional 30 min to complete exfoliation and dispersion. Subsequently, 0.05 g of dopamine was added, followed by 60 min of sonication. Then, 10 mL of TRIS aqueous solution (5 mg mL^{-1}) was added, and the pH was adjusted to 8.5 using NaOH solutions (0.5 and 0.1 mol L^{-1}). The solution was stirred continuously at 80 °C for 24 h, enabling *in situ* polymerization of dopamine onto GO sheets to form the GO/PDA composite. After polymerization, 4 mL of the reaction mixture was diluted to 100 mL of ultrapure water and sonicated for 15 min before membrane deposition.

2.4. Deposition of PDA and GO/PDA active layers onto membranes

The active layer was deposited onto commercial membranes using an Amicon 8050 dead-end filtration system (Millipore). Initially, different concentrations of GO/PDA dispersion (5, 10, and 15% v/v in water) were evaluated (Figure 1). Based on visual inspection and stability, the 5% dispersion was selected for subsequent experiments. A total volume of 20 mL of the coating solution was filtered through the membrane under constant pressure using N_2 feed (< 1 psi).

2.5. Preparation of dye solutions and calibration curve

Calibration curves were prepared by serial dilutions of aqueous 10 mg L^{-1} stock solutions of MB and CR. Ten concentrations were prepared for each dye (1.0 - 10.0 mg L^{-1}). All solutions were homogenized and stored until analysis. UV–Vis absorbance measurements were performed using a Cary 60 spectrophotometer (*Agilent*) with a quartz cuvette. For the calibration plot, absorbance values were measured at the maximum absorbance wavelengths for each dye, *i.e.,* 497 nm for CR and 665 nm for MB.

2.6. Membrane characterization

FTIR spectra were obtained using a Bruker Tensor II spectrophotometer equipped with a diamond ATR module, operating from 400 to 2000 cm^{-1}, with a resolution of 4 cm^{-1} and 128 scans. Scanning electron microscopy (SEM) images were acquired using a Carl Zeiss EVO LS15 microscope, using a secondary electron detector to assess surface morphology. Atomic force microscopy (AFM) analyses were conducted using a Nanosurf EasyScan 2 system using tapping mode (probe TAP = 190-6) over an area of 25 µm × 25 µm, with a scan rate of 0.9 s per line and 512 points to obtain roughness and topographic parameters. Image processing was performed using Gwyddion software. Optical images were recorded using a Leica Optical Microscope coupled to a Renishaw InVia Micro-Raman Spectrometer. Water contact angle (WCA) measurements were performed using a homemade setup equipped with a USB digital microscope (Hiview), using a 5 µL droplet to evaluate membrane surface wettability.

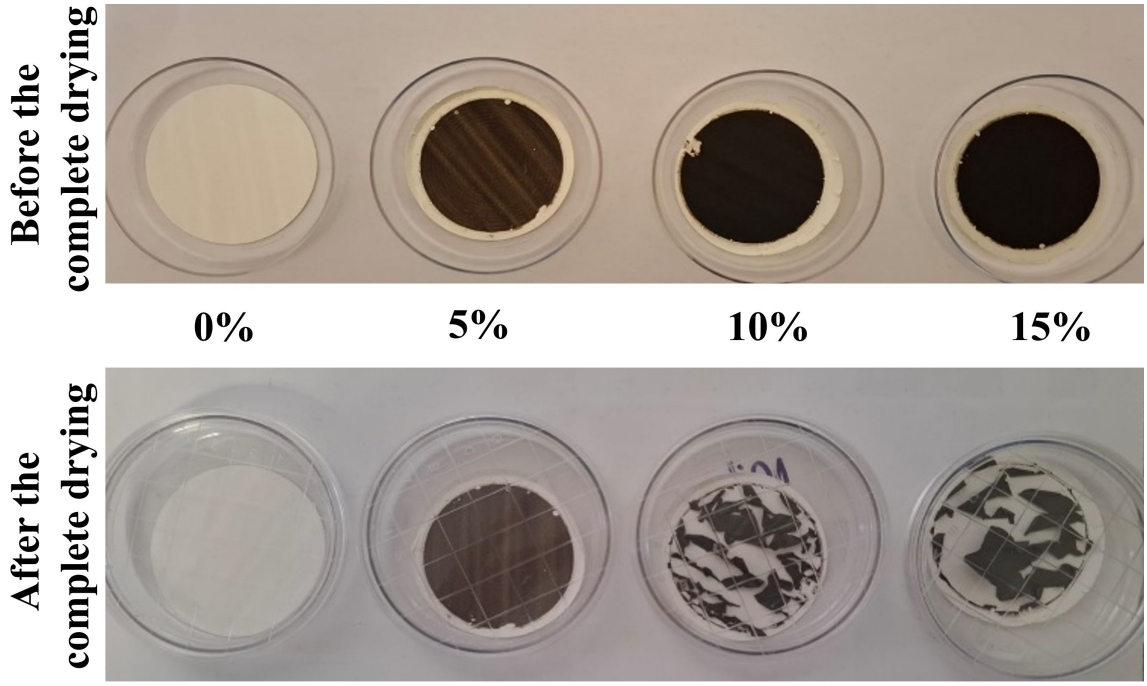

Figure 1. Photographs comparing the membranes modified with different concentrations of GO/PDA (0%, 5%, 10%, and 15%) before and after complete drying at room temperature in a desiccator.

2.7. Filtration experiments

Filtration tests were conducted using an Amicon Stirred Cell dead-end filtration system (model 8050, Millipore from Merck). The membrane was placed in the cell, and 25 mL of dye solution was filtered under constant low pressure using N_2 flow (< 1 psi). After filtration, 2 mL of permeate was collected and analyzed by UV–Vis spectroscopy to determine dye retention by the membrane. All measurements were carried out in triplicate. UV–Vis absorbance measurements were carried out in an Agilent Cary 60 spectrophotometer in the range from 200 to 800 nm using a quartz cuvette and 10 mg L^{-1} dye solutions.

3. Results and discussion

3.1. Membrane characterization

For the initial tests, different concentrations of GO/PDA were deposited onto commercial PVDF membranes (Figure 1) to determine the condition that provides the most suitable coating for the subsequent filtration experiments. The modification process relies on the formation of an active layer on the membrane surface, in which PDA serves as an adhesive matrix, anchoring to the PVDF substrate while simultaneously promoting the incorporation of GO sheets. This results in the development of a thin functional coating capable of altering surface chemistry and morphology[26,27]. By varying the GO/PDA concentration, it is possible to control the thickness, uniformity, and coverage of this layer, which are key factors influencing permeability, selectivity, and overall membrane performance.

As shown in Figure 1, the membranes exhibited noticeable changes in color and surface uniformity as the concentration of the GO/PDA solution used for deposition increased. Prior to drying, samples prepared at higher concentrations (10% and 15%) displayed a darker color, indicating greater material deposition on the membrane surface. However, after complete drying in a desiccator, these membranes demonstrated poor stability, with the GO/PDA active layer rupturing and delaminating. This behavior is likely related to the rigidity of GO sheets, which tend to form more fragile films upon drying[28]. In contrast, the membrane prepared with 5% GO/PDA exhibited a homogeneous, continuous coating with no apparent defects and strong adhesion to the membrane. Therefore, the 5% GO/PDA membrane was used for further characterization and filtration tests.

Morphological characterizations were carried out to observe the influence of the PDA and GO/PDA layers on the membrane surface. Figure 2 reveals gradual changes in the color and surface texture of the membranes. The optical micrograph of the pristine membrane (Figure 2a) exhibits a smooth and homogeneous surface with no visible heterogeneities, which is characteristic of an unmodified PVDF membrane. In the PDA modified membrane (Figure 2b), the optical micrograph reveals lighter regions associated with the deposition of PDA on the PVDF surface. In contrast, the optical micrograph of the GO/PDA membrane (Figure 2c) shows a more opaque and slightly speckled surface, suggesting the formation of a continuous GO/PDA composite layer over the polymeric support. These visual observations confirm the successful formation of coating layers on the modified membranes.

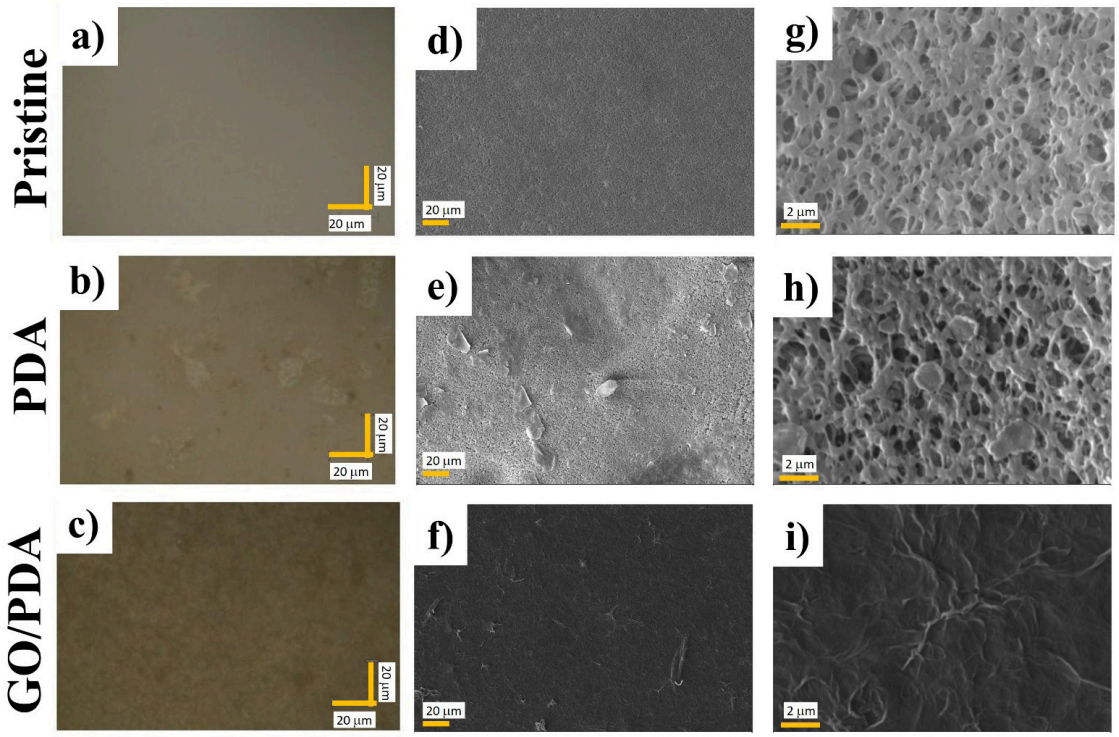

Figure 2. Optical microscopy images obtained using a Leica microscope with a 50× objective: (***a***) pristine membrane; (***b***) membrane modified with PDA; (***c***) membrane modified with GO/PDA. SEM images of the pristine, and PDA and GO/PDA modified membranes, acquired at magnifications of 1,000× (***d–f***) and 20,000× (***g–i***).

SEM images (Figure 2d-i) were obtained to further support the optical microscopy findings. The pristine membrane exhibits a more porous surface with well-defined, homogeneous porosity, typical of PVDF, whereas the PDA membrane shows a partially covered morphology, indicating the presence of a deposited layer. Meanwhile, for the GO/PDA membrane, a broader, smoother surface is observed, with a more compact structure and fewer visible pores, reinforcing the formation of a more continuous film. The formation of a GO layer, which reduces the porosity of filtration membranes, has been reported in the literature, mainly due to its sheet-forming ability, arising from its original two-dimensional atomic structure and the oxidation process that preserves this planar configuration[19,26].

The PDA coating tends to reduce surface roughness and alter the porous structure through surface polymerization and the formation of material aggregates[29,30]. Meanwhile, the presence of GO contributes to the formation of a thicker and more stable film, as its two-dimensional sheets act as barriers and promote better interconnection between coated regions[19,26].

In this sense, AFM analyses (Figure 3a-f) were performed to evaluate the surface topography, while the corresponding roughness parameters are presented in Table 1, for the pristine membrane and those modified with PDA and GO/PDA.

The PDA-modified membrane showed a significant increase in roughness compared to the pristine membrane, indicating the formation of a heterogeneous, irregular layer on the PVDF support. The increase in R*q* and R*a* values indicates that PDA deposition induces pronounced morphological changes, driven by surface polymerization and material accumulation. In addition, the higher values of maximum height (R*h*) and valley depth (R*v*) suggest that the increase in surface roughness parameters reflects a greater amplitude of surface irregularities, resulting in more pronounced peaks and valleys, which can be associated with aggregate formation, as observed in SEM images. This morphology can enhance coating adhesion by increasing the effective contact area and promoting mechanical interlocking between the coating and the substrate[31]. In contrast, the GO/PDA membrane showed a marked reduction in roughness compared to the other membranes, exhibiting a more homogeneous, less irregular surface, as corroborated by the SEM images. This behavior can be attributed to the GO layer, whose planar sheets tend to fill the irregularities created by the PDA, resulting in a smoother, more uniform surface. Although the GO/PDA membrane exhibited lower average roughness parameters (R*a* and R*q*), the R*p*, R*v*, and R*h* values indicate the presence of localized topographical features. This suggests that GO sheets act as a surface-leveling agent over most of the membrane area while still generating isolated peaks and valleys associated with sheet stacking or aggregation.

Figure 3g-i presents the water contact angle measurements for the pristine, PDA, and GO/PDA membranes. The water droplet on the pristine membrane exhibits a more spherical shape and a higher contact angle (67.1°), reflecting the hydrophobic nature of the PVDF membrane.

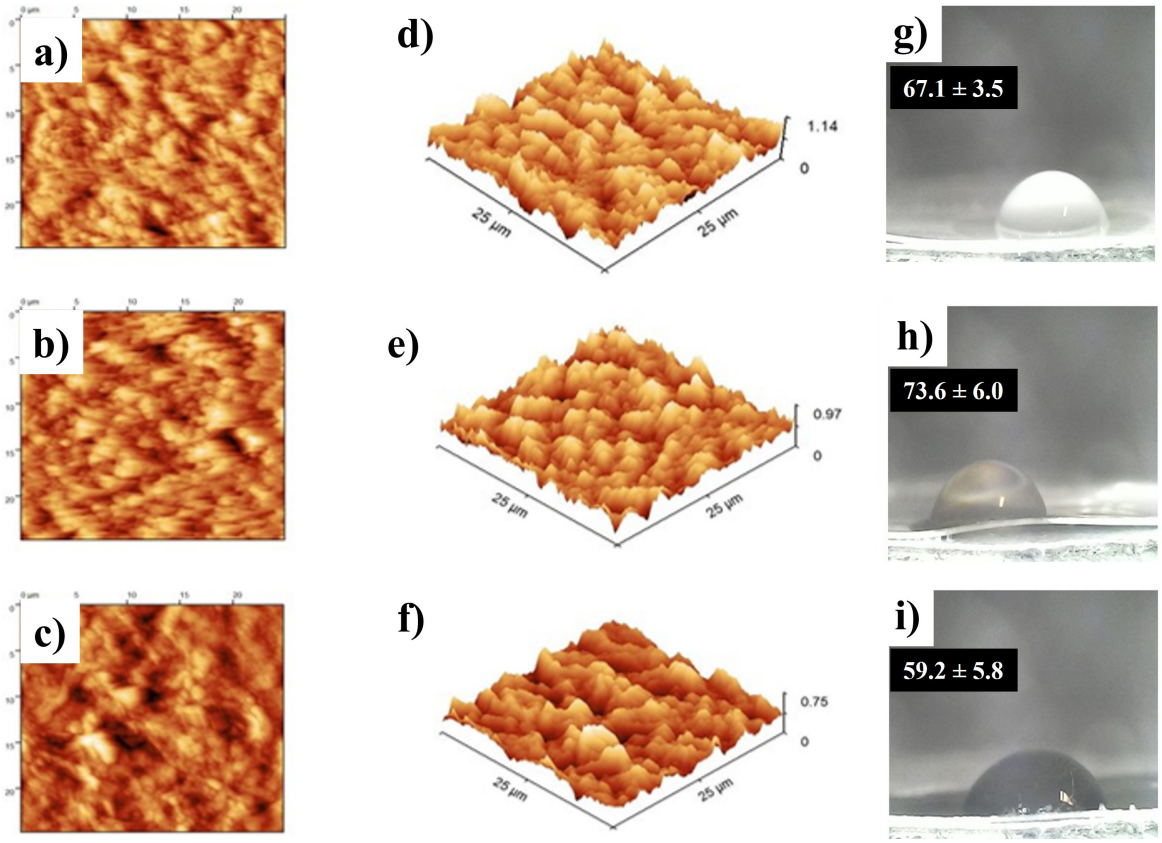

Figure 3. 2D (***a–c***) and 3D (***d–f***) AFM images of the pristine membrane, PDA, and GO/PDA membranes, obtained in tapping mode (probe TAP = 190-6) over an area of 25 µm × 25 µm, with a scan rate of 0.9 s per line and 512 points. (***g-i***) presents the water contact angle measurements of the pristine, PDA, and GO/PDA membranes, highlighting the changes in contact angle after surface modification.

Table 1. Parameters obtained by AFM for the pristine membrane, PDA membrane, and GO/PDA membrane: root mean square roughness (R*q*), average roughness (R*a*), maximum peak height (R*p*), maximum valley depth (R*v*), and maximum height (R*h*).

Membrane	R*q*, nm	R*a*, nm	R*p*, nm	R*v*, nm	R*h*, nm
Pristine	175.7	139.7	769.3	603.1	1372.4
PDA	349.6	216.1	2385.6	733.0	3118.6
GO/PDA	91.8	75.0	143.9	236.9	380.9

This behavior is associated with the presence of fluorinated groups, which have low polarity and reduce surface energy, thereby limiting water–surface interactions[32]. After PDA deposition, a slight increase in the contact angle (73.6°) is observed, which can be attributed to an increase in surface roughness of the membrane, described by the Wenzel model[33]. In contrast, the GO/PDA-modified membranes exhibited a reduced contact angle of 59.2°, decreasing the hydrophobic character of the membrane due to the presence of oxygen-functional groups on its basal plane and edges of the nanosheets[34]. GO coatings have been investigated to improve the hydrophilicity of various surfaces, such as polymers[35] and ceramics[36].

The pristine membrane exhibited the main IR bands of PVDF (Figure 4). The bands at 483 and 510 are associated with the CF_2 wagging and CF_2 bending vibrations, respectively[37]. The bands at 764 and 614 cm^{-1} are attributed to the rocking vibrations (mixed mode of CF_2 bending and CCC skeletal vibration)[38]. 840 cm^{-1} band is assigned to the mixed mode of CH_2 rocking and CF_2 asymmetric stretching[37,38]. The band at 874 cm^{-1} was attributed to C–C skeletal vibration[39,40] as well as CF_2 symmetric stretching[41]. The band at 1402 cm^{-1} is assigned to combined CH_2 wagging and to C–C asymmetric stretching vibrations[37]. The band at 1174 cm^{-1} corresponds to the combination of CF_2 asymmetric stretching, CF_2, and CH_2 rocking vibrations[37].

After PDA deposition, no significant shifts in the position of the PVDF bands were observed. However, a discrete band appeared at ~1613 cm^{-1}, which is attributed to the overlap of aromatic C=C resonance vibrations and N–H bending vibrations[42], as found in other PDA and PVDF formulations[42-44]. In addition, a broad band between 3200 and 3500 cm^{-1} is assigned to N–H and O–H stretching vibrations in PDA[43].

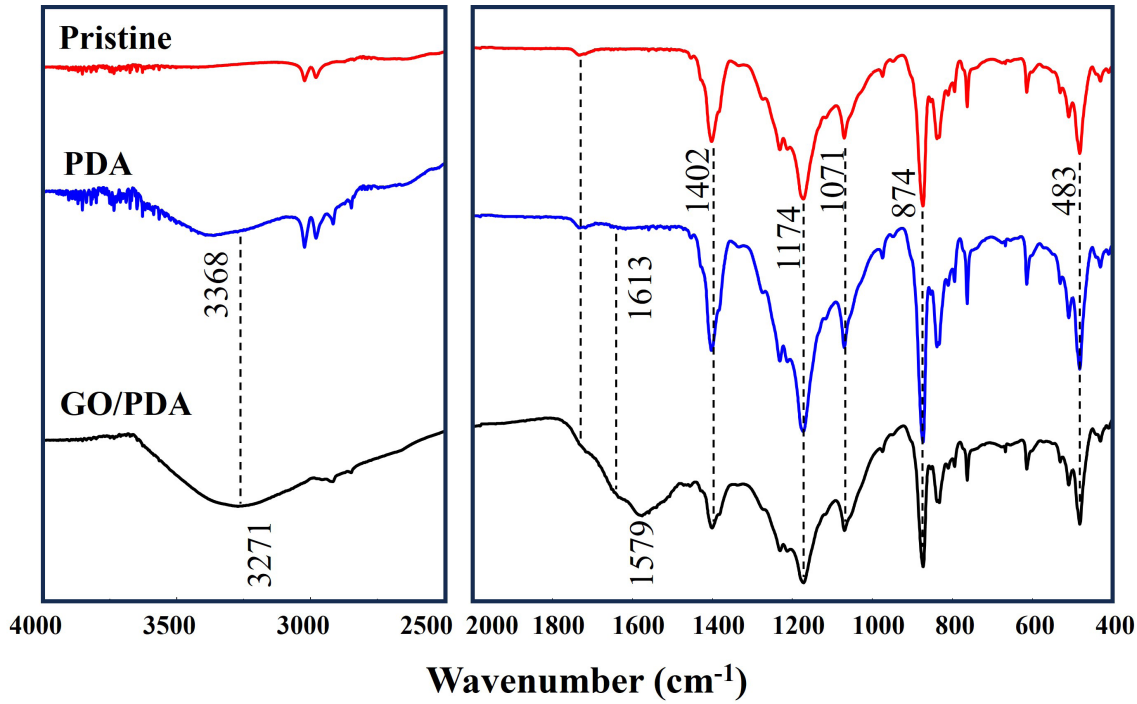

Figure 4. FTIR spectra of pristine PVDF membrane and modified PVDF membranes with PDA and GO/PDA.

Upon modification with GO/PDA, a broad band appeared in the region between 1480 and 1730 cm^{-1}, resulting from the overlap of GO bands with those of PVDF and PDA. The most prominent bands of GO are typically located at ~1720 cm^{-1} (C=O stretching), ~1620 cm^{-1} (water molecules) and ~1580 cm^{-1} (aromatic C=C bonds)[45]. A broad band associated with O–H vibrations is also observed in ~3700 – 3000, which is attributed to hydroxyl groups from carboxyl functionalities and to residual water intercalated within the GO structure[46] overlapped with the PDA N–H and O–H stretching vibrations. Another noticeable feature is the increase in the relative intensity of the band at 1174 cm^{-1} (PVDF 874 cm^{-1} band as reference) due to the additional contribution from C–O stretching vibrations (epoxy groups) of GO[45].

3.2. Filtration tests and dye-membrane interaction investigation

After characterizing the membranes, filtration tests were performed using the pristine membrane, the PDA-modified membrane, and the GO/PDA-modified membrane. Figure 5a illustrates the spectra of the CR dye at various concentrations to construct the calibration plot (Figure 5b), presenting a maximum absorbance at 497 nm, which corresponds to the π–π* electronic transition of free electron pairs of the N atoms of the azo groups associated with the dye structure[47]. The linear regression is presented in Figure 5b, reaching a coefficient of determination (R^2) of 0.99349, indicating an excellent correlation between concentration and absorbance.

Figure 5c shows the absorption spectra of the filtrate for all membranes, whose absorbance was used for the dye retention calculations. Retention values for CR through the filters were relatively low, reaching 9.78% and 7.12% for the PDA-modified and the GO/PDA-modified membranes, respectively (Figure 5d). However, the unmodified membrane exhibited the highest retention, reaching 12.02%. Despite this slightly higher performance, the pristine membrane still showed limited ability to retain CR.

In this sense, the dye-membrane interaction was investigated (Figure 6). In the case of CR, almost no significant differences are observed between the FTIR spectra of PDA-modified membrane and GO/PDA-modified membrane before and after filtration. Only an increase in the relative intensity of the band at 1071 cm^{-1} is observed, which was caused by the overlap of the CR sulphonic group vibration[48]. In addition, a discrete attenuation of the bands associated with GO is noted, as evidenced by the decrease in the relative intensity ratios I_{1580}/I_{483} and I_{1634}/I_{483}, due to the dye adsorption. Considering that CR carries a negative charge at the working pH of ~5.0 (pH > pI), as well as GO and PDA, electrostatic interactions are unfavorable. Therefore, the interactions may occur governed by hydrogen bonding (CR contains amine groups, GO contains hydroxyl groups, and PDA contains both amine and hydroxyl groups) and by π–π interactions between aromatic rings[49].

After evaluating the anionic CR, the cationic MB was also evaluated. Figure 7a shows the spectra of the MB solutions at various concentrations used to construct the calibration curve, which exhibits a maximum absorbance at 665 nm, corresponding to the n–π* and π–π* transitions (hypochromic and bathochromic shifts, respectively)[50]. As observed for the CR, the linear regression for the MB dye is shown in Figure 7b. The coefficient of determination obtained for MB was 0.99928, indicating high linearity between absorbance and dye concentration.

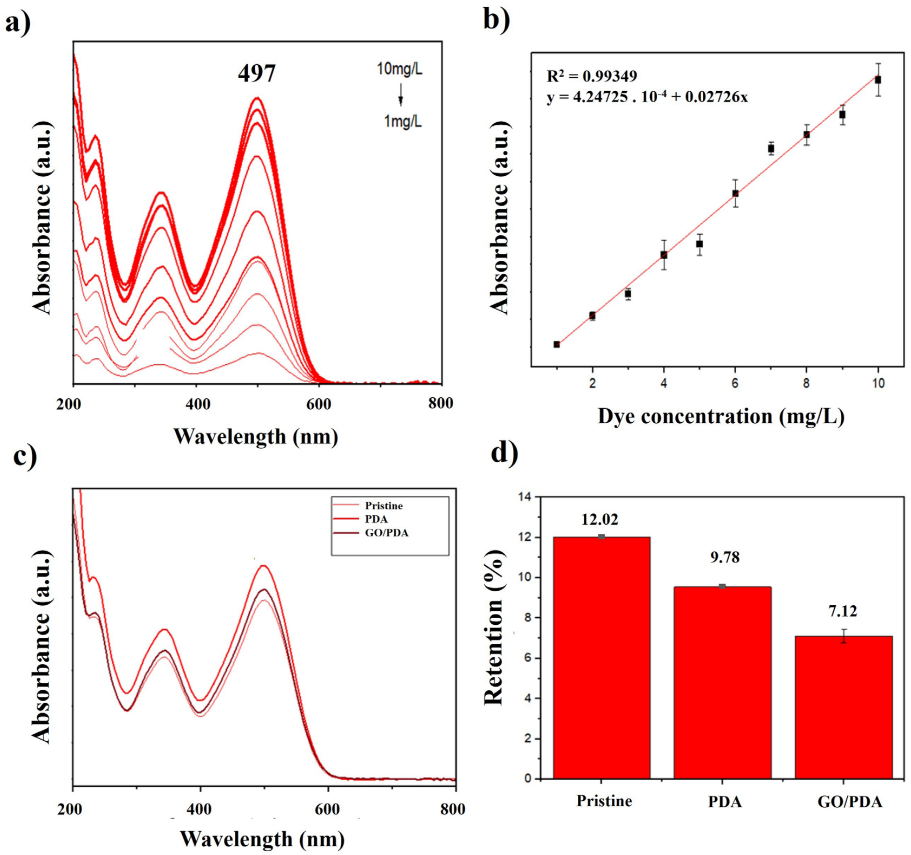

Figure 5. *(a)* Absorbance spectra of CR dye at different concentrations (1 to 10 mg L^{-1}), obtained by UV-Vis spectroscopy, *(b)* Corresponding calibration curve, fitted by linear regression model, used to calculate the concentrations in the filtration steps, *(c)* Absorbance spectra obtained for CR dye after filtration (initial concentration of 10 mg L^{-1}) in pristine membranes, in PDA-modified membrane and with GO/PDA-modified membrane. *(d)* Percentage of CR retention for each membrane.

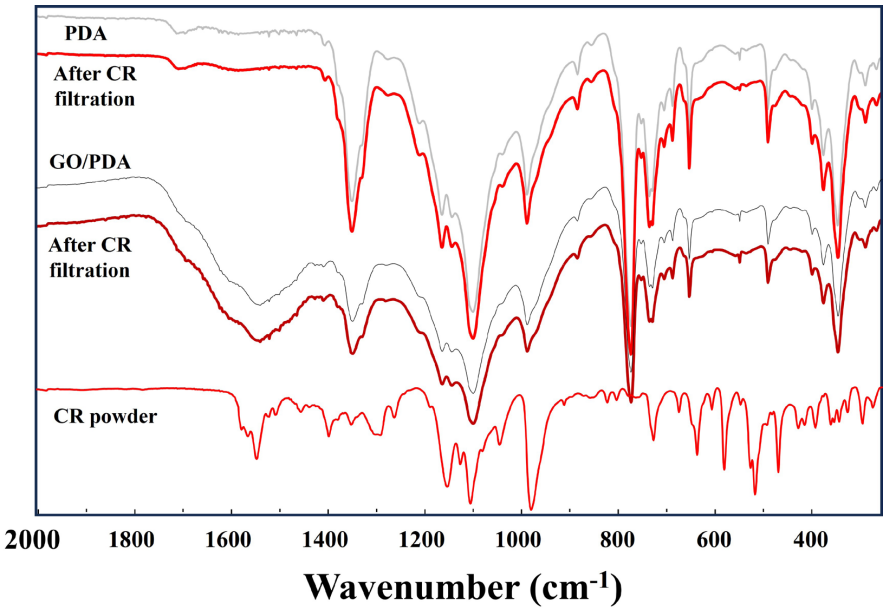

Figure 6. FTIR spectra of PDA and GO/PDA-modified membranes before and after filtration of CR solution. The CR powder spectrum is presented as a reference.

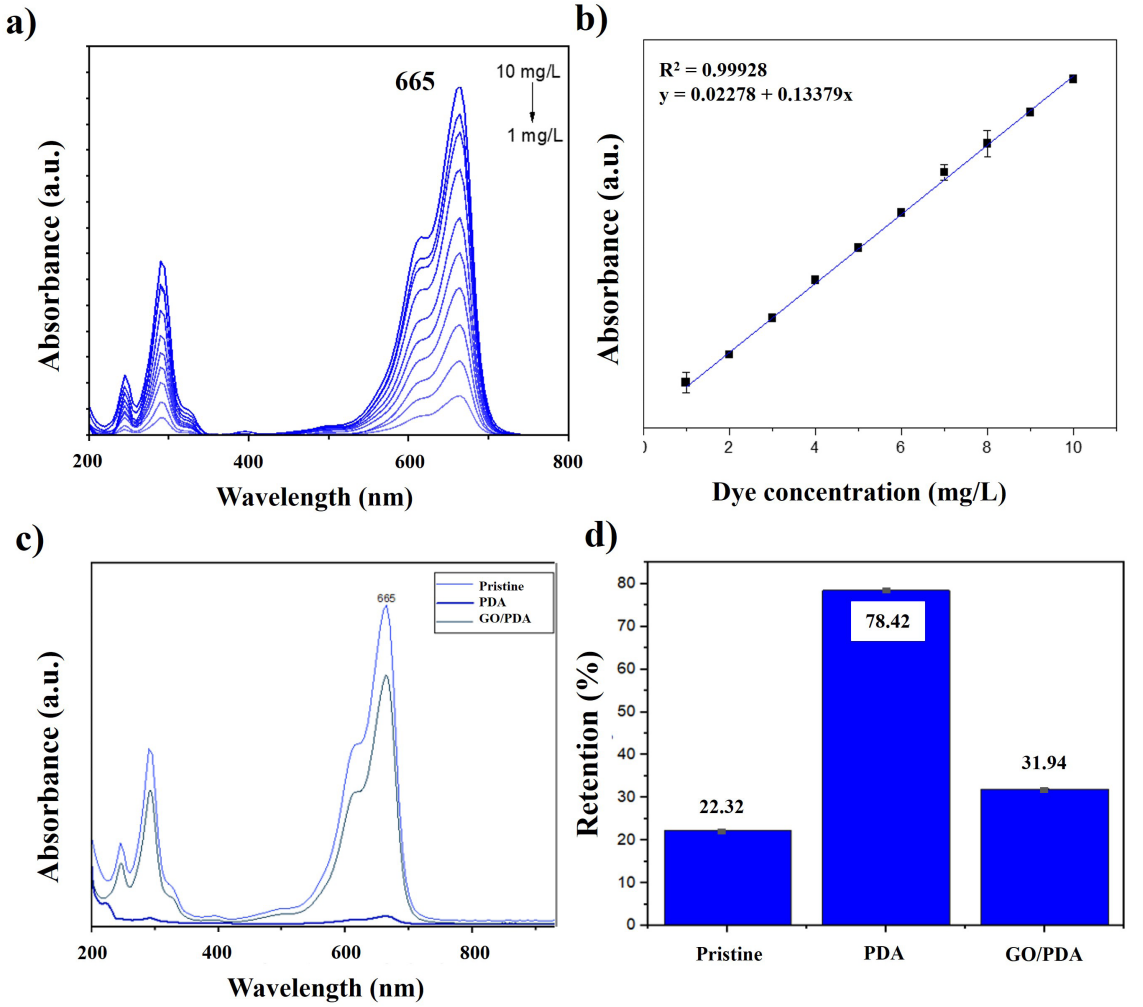

Figure 7. ***(a)*** Absorbance spectra of MB dye at different concentrations (1 to 10 mg/L), obtained by UV-Vis spectroscopy, and ***(b)*** corresponding calibration curve, fitted by linear regression model, used to calculate the concentrations in the filtration steps, ***(c)*** Absorbance spectra obtained for MB dye after filtration (initial concentration of 10 mg L^{-1}) in pristine membranes, in PDA-modified membrane and GO/PDA-modified membrane. ***(d)*** Percentage of MB retention for each membrane.

Figure 7c presents the absorption spectra of the filtrate for all membranes, while Figure 7d shows the retention results, which reached 78.42% for the PDA membrane, 31.94% for the GO/PDA membrane, and 22.32% for the pristine membrane, confirming that the charge of the contaminant plays an important role in the retention process. Thus, it can be observed that the membrane modified with PDA exhibited higher MB retention efficiency, whereas the presence of GO reduced it.

PDA contains a variety of functional groups, such as amines and catechols, which provide multiple interaction sites and favor electrostatic and π–π interactions with cationic molecules[27,30]. Therefore, the higher density of reactive groups in PDA contributes to the intense adsorption of MB on the membrane surface. On the other hand, the behavior under GO/PDA-modified membranes suggests that GO acts as a limiting factor for dye adsorption, possibly by affecting the availability of active groups of the PDA coating. Overall, MB results indicate a higher filtration capacity than CR across all evaluated membranes. This difference may be associated with the electrical charge of the dyes, highlighting that the modified membranes exhibit improved retention of cationic dyes, whereas retention of anionic dyes is less pronounced[51].

After MB filtration, the FTIR spectra presented minor changes (Figure 8). At the experimental pH used in this study (natural pH ~ 5.0), MB carries a positive charge (pKa = 2.6)[52], whereas PDA and GO exhibit negative charges (isoelectric point of PDA (pI_{PDA}) = 4.0[53]), which would favor electrostatic interactions between the dye and the membranes. In addition, both MB and the membrane components (PDA and GO) contain structures rich in conjugated C=C bonds, which would facilitate π–π interactions. In the spectra of PDA and GO/PDA-modified membranes after the MB filtration, the most intense MB band (1600 cm^{-1}) was found accompanied by slight shifts, indicating changes in the stretching energies of the C=C and C=N bonds[54,55].

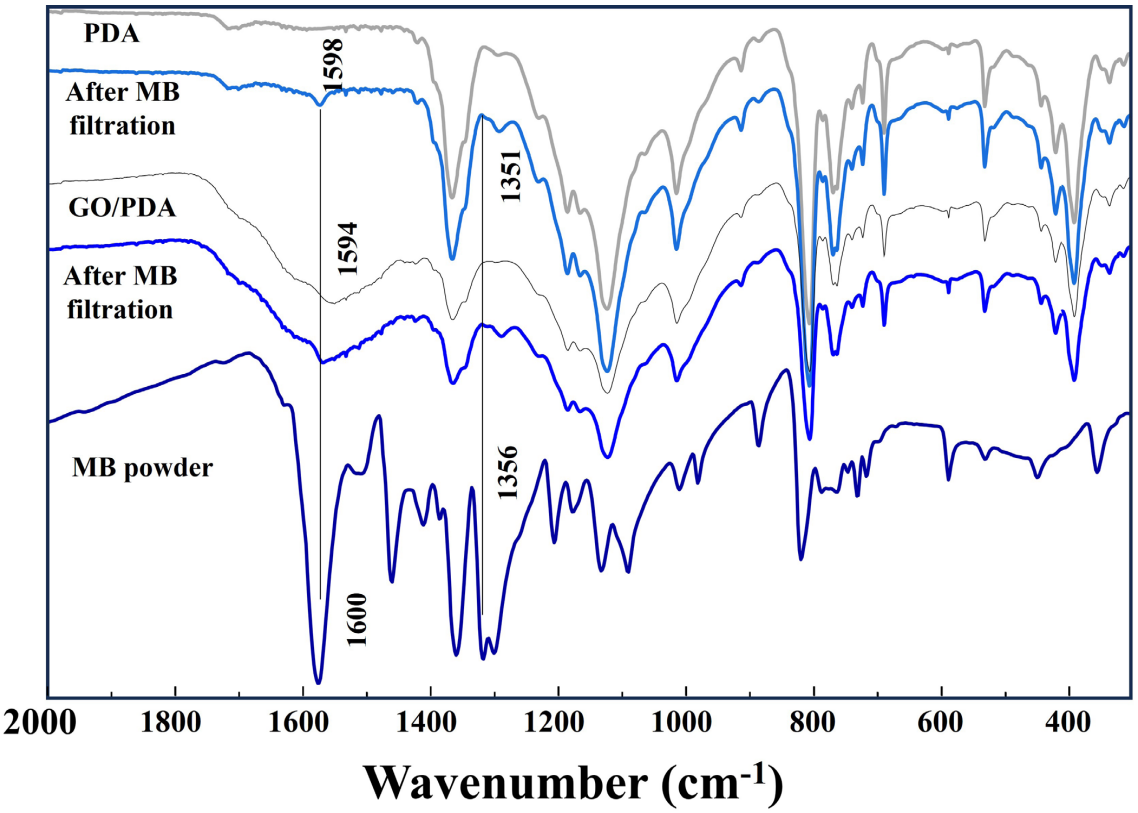

Figure 8. FTIR spectra of PDA and GO/PDA-modified membranes before and after filtration of MB solution. MB powder spectrum is presented as a reference.

A closer inspection also reveals the presence of the band associated with the C=S$^+$ group[54,55] (1356 cm^{-1} in the MB spectrum), which appears shifted to 1352 cm^{-1} (more readily observed in the GO/PDA membrane spectrum), suggesting a possible electrostatic interaction. Therefore, both π–π and electrostatic interactions may contribute to the interaction between MB and the membranes.

It is important to note that both membrane surface charge and dye ionization are strongly dependent on solution pH[56]. Variations in pH can alter the protonation or deprotonation of functional groups present on the PDA and GO/PDA coatings, thereby modifying electrostatic interactions with dye molecules. Likewise, changes in the ionization state of MB and CR may influence their aggregation behavior, adsorption affinity, and retention during filtration[57,58]. In the present study, filtration experiments were conducted at the natural pH of the dye solutions (approximately pH 5.0) in order to better simulate practical treatment conditions and avoid additional pre-treatment steps. Although pH optimization may further affect membrane performance, the results obtained under natural conditions provide a realistic assessment of the separation process.

Figure 9 presents the retention results for MB and CR in a mixed solution (1:1, 10 mg/L each dye), used to evaluate membrane selectivity toward compounds with opposite charges.

Unlike the retention of individual dyes, which showed low retention, when the mixture was evaluated, CR dye exhibited higher retention across all analyzed membranes. In contrast, the retention of the cationic dye MB was lower, except for the PDA-modified membrane, in which the CR and MB were retained at similar levels. These findings confirm that surface modifications directly influence membrane selectivity.

Overall, the retention behavior suggests that the coexistence of both dyes in the mixture influenced the dye retention capacity. Similar behavior has been reported in adsorption studies involving MB and CR, where an increased dye uptake is observed in mixed solution[59,60]. This increase can be explained by the interactions between CR and MB. The presence of adsorbed MB may facilitate the formation of mixed MB–CR supramolecular assemblies via electrostatic attraction, hydrogen bonding, and aromatic stacking interactions, thereby increasing the effective size of the retained species.

In contrast, the GO/PDA membrane showed a significant reduction in MB retention (approximately 20%) and intermediate CR performance (approximately 70%). This difference suggests selective behavior, with a greater affinity for the CR dye in the mixture. This is because the CR exhibits a stronger tendency toward aggregation compared to MB, forming supramolecular assemblies driven predominantly by π–π stacking interactions between the extended aromatic rings. These interactions promote the formation of ordered, ribbon-like or stacked structures in solution, which can further evolve into larger aggregates depending on concentration, ionic strength, and pH[61].

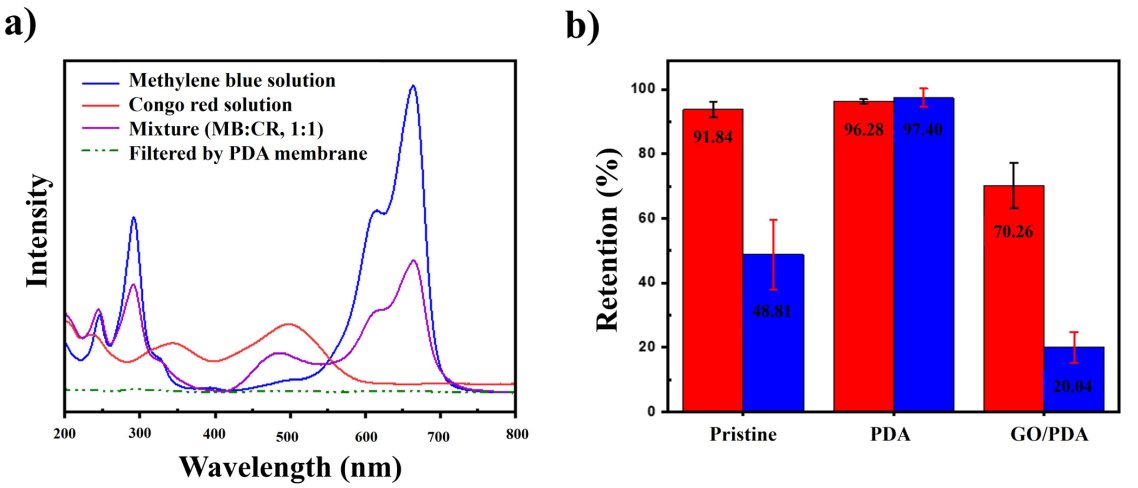

Figure 9. ***(a)*** UV–Vis absorption spectra of MB (blue line) and CR (red line) dyes (both 10 mg L^{-1}), the 1:1 mixture (purple line), and the mixed solution after filtration through the PDA coated membrane (green dashed line). ***(b)*** Comparative bar chart showing the percentage retention (%) of MB (10 mg L^{-1}) and CR (10 mg L^{-1}) in a mixed solution (1:1) after filtration through the pristine, PDA and GO/PDA-modified membranes.

Table 2. Retention value of each dye in the mixture test and the calculated selectivity factor.

Membrane	CR retention	MB retention	Selectivity factor
Pristine	91.84	48.81	1.88
PDA	96.28	97.40	0.99
GO/PDA	70.26	20.04	3.50

In contrast, MB predominantly undergoes a simpler, well-defined monomer–dimer equilibrium, with aggregation typically limited to dimers or small oligomers under conventional conditions[62]. As a result, CR (anionic dye) aggregates tend to be more stable and persistent in solution, whereas MB (cationic dye) remains dynamically distributed between monomeric and dimeric forms[63]. Thus, the passage of CR through the less porous surfaces, such as GO/PDA membranes, is more difficult.

To further quantify the selective retention behavior observed in the mixed-dye experiments, a selectivity factor ($S_{CR/MB}$) was calculated as the ratio between the retention of CR and MB, according to Equation 1 adapted from Schirg and Widmer[64]:

$$S_{CR/MB} = \frac{R_{CR}}{R_{MB}} \quad (1)$$

where R_{CR} and R_{MB} correspond to the retention percentages of congo red and methylene blue, respectively. A selectivity factor equal to 1 indicates similar retention of both dyes, whereas values greater than 1 indicate preferential retention of CR.

The calculated values revealed distinct separation behaviors among the membranes (Table 2). The PDA-coated membrane exhibited a selectivity factor close to unity (0.99), indicating a non-selective removal process in which both dyes were efficiently retained. In contrast, the GO/PDA membrane showed a considerably higher selectivity factor (3.50), confirming its preferential retention of CR over MB. This result demonstrates that the incorporation of graphene oxide not only modifies the membrane morphology but also promotes a more selective separation mechanism when oppositely charged dyes are present simultaneously.

Although the incorporation of GO improved the selective retention of CR in mixed-dye systems ($S_{CR/MB}$ = 3.50), this enhancement was accompanied by a reduction in the overall retention efficiency, particularly for MB alone (from 78.42% without GO to 31.94% with GO) and MB in the mixture (from 97.40% without GO to 20.04% with GO). This behavior highlights a common trade-off in membrane design, where increased selectivity is often achieved at the expense of total contaminant removal. In the present study, the PDA-coated membrane exhibited superior overall dye retention, whereas the GO/PDA membrane demonstrated a greater ability to discriminate between dyes with different physicochemical characteristics. Therefore, the choice between PDA and GO/PDA modifications should ultimately depend on the intended application, whether the primary objective is maximum dye removal or selective separation. Thus, a staged membrane configuration combining PDA-coated and GO/PDA membranes in separate modules could be envisioned to integrate high overall dye removal with selective separation, although further optimization would be required to mitigate the loss in total retention associated with GO incorporation.

3.3. Comparison with the literature

Recent literature has highlighted the versatility of filtration membranes incorporating GO and its derivatives.

Table 3. Literature data for GO-based membranes to remove contaminants from water.

Membrane	Contaminant	Preparation method	Filtration method/system	Retention capacity	Ref
PDA and GO/PDA modified PVDF membrane	CR and MB dyes and its mixture	Deposition by filtration assembly	Dead-end system	>70% of MB	***This study***
PDA modified PVDF membrane	CR and MB dyes and its mixture	Deposition by filtration assembly	Dead-end system	>96% of CR and >97% of MB for the mixture	***This study***
Ferrous oxide/ graphene oxide catalytic membranes	Haloacetic acids and chlorinated organic pollutants	GO nanosheets deposited by simple *in-situ* growth and filtration assembly	Continuous flow under pressure	≈ 100%	[65]
MOF-intercalated GO membranes	Organic pollutants and salts	Incorporating an appropriate amount of ZIF-8 into the GO-based active layer	Nanofiltration in crossflow (tangential flow) operation	98 ± 2% for diclofenac	[66]
Nanocomposite membrane of graphene oxide and cellulose nanocrystals (extracted from bananas)	Cr^{3+}, Co^{2+}, Ni^{2+}, Pb^{2+}, Cd^{2+} and Methylene blue	casting	Vacuum filtration	For Cd^{2+} and Pb^{2+}, around 99%. For MB 100%	[67]
Graphene oxide (GO)-polyvinyl alcohol (PVA) membrane	High-density polyethylene (HDPE)-based microplastics	GO layers were deposited on a substrate via vacuum filtration	Vacuum filtration	95%	[68]
Polyethersulfone membranes modified with polyvinyl alcohol (PVA) and graphene oxide (GO)	Sunset yellow (SY)	Layer-by-layer self-assembly method	Pressurized filtration	~99.9	[69]
Aminated graphene oxide (NH_2-GO)-based PVDF membranes	MB and methyl orange	Phase-inversion method	Nanofiltration in crossflow (tangential flow) operation	96.6% for methylene blue and 88.5% for methyl orange	[70]
Polyethersulfone-graphene oxide (PES-GO)	Turbidity, color, Abs254, COD, DOC, proteins and carbohydrates	Phase-inversion method	Direct membrane filtration (DMF)	99% for carbohydrates	[71]
Oxidized carbon nanotube intercalated nitrogen doped reduced graphene oxide	4-chlorophenol	Mixing, filtering, compaction	Dead-end filtration system	100% of 4-chlorophenol removal	[72]
Reduced graphene oxide (S-rGO) membrane	Na_2SO_4, $MgSO_4$, NaCl, $MgCl_2$	Vacuum filtration	Self-designed dead-end filtration device	For Na_2SO_4 the rejection was up to 91.6%	[73]

Different incorporation strategies, resulting in distinct membrane architectures, enable its role in the retention of a wide range of organic and inorganic contaminants. In this context, Table 3 provides a comparative overview of the literature, summarizing GO-based membranes, their fabrication methods, the target contaminants, and their retention performance.

In this study, the retention of the dyes evaluated individually was relatively low, particularly for CR. However, when tested as a mixed solution, a significant improvement in retention was observed for CR, reaching approximately 97% for the PDA-modified membrane. For comparison, the GO/PDA membrane exhibited CR retention of approximately 70%. Although the retention values obtained in this work are lower than those reported in the studies summarized in Table 3, the GO/PDA membrane demonstrated a distinct selective behavior toward the evaluated dyes. This feature represents a key distinction from the other studies, where selectivity between dyes was not clearly observed.

4. Conclusion

The modification of commercial PVDF membranes with polydopamine (PDA) and with the graphene oxide/ polydopamine (GO/PDA) composite proved to be an effective strategy for altering surface properties and filtration behavior. The analyses confirmed that the PDA coating increased membrane hydrophobicity and surface reactivity, while GO incorporation enhanced hydrophilicity and led to a more stable, homogeneous surface.

In the filtration tests, the membrane modified only with PDA showed the highest MB removal efficiency, exceeding 78%. In contrast, the presence of GO partially reduced this efficiency, possibly due to a lower exposure of PDA amine

groups on the membrane surface. For CR, retention rates were lower, possibly due to repulsion between the anionic dye molecules and the oxygenated groups on the modified membrane surfaces.

Overall, the evaluation of the mixture revealed a synergistic effect, likely arising from interactions between MB and CR, which increased dye retention compared to the single-dye system. In this sense, PDA modification enhances the retention of both dyes, while GO mainly contributes to improving filtration selectivity among the evaluated dyes, which can be associated with the aggregation properties of the dyes. Hence, PDA modification shows promising potential to improve the performance of PVDF membranes in nanofiltration processes for the removal of MB from aqueous media, while GO/PDA-modified membranes demonstrate great potential for selective retention of the evaluated dyes (with a selectivity factor of 3.50). These findings highlight the potential of surface-engineered PVDF membranes as tunable platforms for dye separation, while also indicating that further optimization of the coating architecture, GO content, and exposure of PDA functional groups may enhance retention efficiency and selectivity in more complex aqueous systems.

5. Acknowledgments

The authors would like to thank the Brazilian funding agencies São Paulo Research Foundation - FAPESP (#2018/22214-6, #2021/14235-6, and #2025/01226-0), CNPq (#445991/2024-0, #302465/2025-1, #407863/2023-0), CAPES (#001), INCT/INEO/FAPESP (2025/27044-5) and PIBIC/UNESP/CNPq for the financial support. We would also like to thank LabMMEV- FCT/UNESP for the SEM image.

6. Data Availability

All the data supporting the results of this study is available upon request to the corresponding author upon reasonable request.

7. References

1. Pervez MN, Mondal IH, Cai Y, Zhao Y, Naddeo V. Textile waste management and environmental concerns. In: Ibrahim I, Mondal H, editor. Fundamentals of natural fibres and textiles. Duxford: Woodhead Publishing; 2021. p. 719-39. https://doi.org/10.1016/B978-0-12-821483-1.00002-4.
2. Grand View Research, Inc. Textile market size, share & growth [Internet]. San Francisco: Grand View Research; 2025 [cited 2025 Dec 17]. (Industry Report; 2033). Available from: https://www.grandviewresearch.com/industry-analysis/textile-market
3. Oliveira GCO No, Silva PC, Tucci HNP, Amorim M. Reuse of water and materials as a cleaner production practice in the textile industry contributing to blue economy. J Clean Prod. 2021;305:127075. https://doi.org/10.1016/j.jclepro.2021.127075.
4. Leal Filho W, Dinis MAP, Liakh O, Paço A, Dennis K, Shollo F, et al. Reducing the carbon footprint of the textile sector: an overview of impacts and solutions. Text Res J. 2024;94 (15-16):1798-814. https://doi.org/10.1177/00405175241236971.
5. Mehta M, Sharma M, Pathania K, Jena PK, Bhushan U. Degradation of synthetic dyes using nanoparticles: a mini-review. Environ Sci Pollut Res Int. 2021;28(36):49434-46. https://doi.org/10.1007/s11356-021-15470-5.
6. Lin J, Ye W, Xie M, Seo DH, Luo J, Wan Y, et al. Environmental impacts and remediation of dye-containing wastewater. Nat Rev Earth Environ. 2023;4(11):785-803. https://doi.org/10.1038/s43017-023-00489-8.
7. Islam T, Repon M, Islam T, Sarwar Z, Rahman MM. Impact of textile dyes on health and ecosystem: a review of structure, causes, and potential solutions. Environ Sci Pollut Res Int. 2023;30(4):9207-42. https://doi.org/10.1007/s11356-022-24398-3.
8. Mohammed S. Graphene oxide: A mini-review on the versatility and challenges as a membrane material for solvent-based separation. Chem Eng J Adv. 2022;12:100392. https://doi.org/10.1016/j.ceja.2022.100392.
9. Foorginezhad S, Zerafat MM, Ismail AF, Goh PS. Emerging membrane technologies for sustainable water treatment: a review on recent advances. Environ Sci Adv. 2025;4(4):530-70. https://doi.org/10.1039/D4VA00378K.
10. Namla D, Oves M, Alshaeri MA, Al-Maaqar SM, Issa HNY, Mangse G. Nanofiltration as an advanced wastewater treatment technique: a comprehensive review. Discov Appl Sci. 2025;7(4):355. https://doi.org/10.1007/s42452-025-06576-3.
11. Liu M, Yu F, Niu L, Chi H. Advances in nanofiltration membrane pore size adjustment techniques: A review. Environmental Functional Materials. 2025;4(1):65-78. https://doi.org/10.1016/j.efmat.2025.02.002.
12. Suhalim NS, Kasim N, Mahmoudi E, Shamsudin IJ, Mohammad AW, Mohamed Zuki F, et al. Rejection mechanism of ionic solute removal by nanofiltration membranes: an overview. Nanomaterials. 2022;12(3):437. https://doi.org/10.3390/nano12030437.
13. Mannaf MM, Rahman MM, Sabuj ST, Talukder N, Lee ES. Current progress in advanced functional membranes for water-pollutant removal: a critical review. Membranes. 2025;15(10):300. https://doi.org/10.3390/membranes15100300.
14. Hadi MK, Wang X, Peng Y, Sangaraju S, Ran F. Functional polymeric membrane materials: a perspective from versatile methods and modification to potential applications. Polym Sci Technol. 2025;1(5):366-412. https://doi.org/10.1021/polymscitech.4c00030.
15. Rana D, Matsuura T. Surface modifications for antifouling membranes. Chem Rev. 2010;110(4):2448-71. https://doi.org/10.1021/cr800208y.
16. Ebrahimi M. Innovative physical and chemical strategies for the modification and development of polymeric microfiltration membranes: a review. Polymers. 2026;18(3):311. https://doi.org/10.3390/polym18030311.
17. Bonyadi E, Ashtiani FZ, Ghorabi S, Niknejad AS. Bio-inspired hybrid coating of microporous polyethersulfone membranes by one-step deposition of polydopamine embedded with amino-functionalized SiO_2 for high-efficiency oily wastewater treatment. J Environ Chem Eng. 2022;10(1):107121. https://doi.org/10.1016/j.jece.2021.107121.
18. Yang W, Zhao Z, Pan M, Gong L, Wu F, Huang C, et al. Mussel-inspired polyethylene glycol coating for constructing antifouling membrane for water purification. J Colloid Interface Sci. 2022;625:628-39. https://doi.org/10.1016/j.jcis.2022.06.038.
19. Tiwary SK, Singh M, Chavan SV, Karim A. Graphene oxide-based membranes for water desalination and purification. NPJ 2D Mater Appl. 2024;8(1):27. https://doi.org/10.1038/s41699-024-00462-z.
20. Nain A, Sangili A, Hu SR, Chen C, Chen Y, Chang H. Recent progress in nanomaterial-functionalized membranes for removal of pollutants. iScience. 2022;25(7):104616. https://doi.org/10.1016/j.isci.2022.104616.
21. Vo TS, Lwin KM, Kim K. Recent developments of nano-enhanced composite membranes designed for water/wastewater purification: a review. Adv Compos Hybrid Mater. 2024;7(4):127. https://doi.org/10.1007/s42114-024-00923-5.
22. Buya DG, Aflaha R, Rianjanu A. Effect of zeolite mesh size variation on the filtration performance of Zeolite-PAN/PVDF nanofiber for methylene blue dye removal. Greensusmater. 2025;2(1):1-6. https://doi.org/10.62755/greensusmater.2025.2.1.1-6.

23. Deng Z, Shang B, Peng B. Polydopamine based colloidal materials: synthesis and applications. Chem Rec. 2018;18(4): 410-32. https://doi.org/10.1002/tcr.201700051.
24. Chen S, Liu P, Li Z, Bi Y, Li F, Yu Y. Biomimetic mussel technology for membrane material modification: adhesion mechanism and design strategy. J Polym Sci. 2023;1(22): 2815-27. https://doi.org/10.1002/pol.20230205.
25. An Y, Gao X, Jiang W, Han J, Ye Y, Chen T, et al. A critical review on graphene oxide membrane for industrial wastewater treatment. Environ Res. 2023;223:115409. https://doi.org/10.1016/j.envres.2023.115409.
26. Liu Y, Tu W, Chen M, Ma L, Yang B, Liang Q, et al. A mussel-induced method to fabricate reduced graphene oxide/halloysite nanotubes membranes for multifunctional applications in water purification and oil/water separation. Chem Eng J. 2018;336: 263-77. https://doi.org/10.1016/j.cej.2017.12.043.
27. Kumar M, Sreedhar N, Thomas N, Mavukkandy M, Ismail RA, Aminabhavi TM, et al. Polydopamine-coated graphene oxide nanosheets embedded in sulfonated poly(ether sulfone) hybrid UF membranes with superior antifouling properties for water treatment. Chem Eng J. 2022;433(2):133526. https://doi.org/10.1016/j.cej.2021.133526.
28. Vishvanathperumal S, Kannan A. Effect of graphene oxide (GO) on the mechanical properties of ethylene-propylene-diene monomer/acrylonitrile butadiene rubber (EPNBR) blend composites. J Polym Res. 2025;32(4):145. https://doi.org/10.1007/s10965-025-04393-1.
29. Chang ZH, Lyly LHT, Teow YH, Yeap SP, Sum JY. Insight into polydopamine coating on microfiltration membrane with controlled surface pore size for enhanced membrane rejection. Polymer. 2023;287:126446. https://doi.org/10.1016/j.polymer.2023.126446.
30. Lee HA, Ma Y, Zhou F, Hong S, Lee H. Material-independent surface chemistry beyond polydopamine coating. Acc Chem Res. 2019;52(3):704-13. https://doi.org/10.1021/acs.accounts.8b00583.
31. Gent AN, Lin CW. Model studies of the effect of surface roughness and mechanical interlocking on adhesion. J Adhes. 1990;32(2–3):113-25. https://doi.org/10.1080/00218469008030185.
32. Maghami M, Abdelrasoul A. Pair interaction energy decomposition analysis (PIEDA) and experimental approaches for investigating water interactions with hydrophilic and hydrophobic membranes. J Mol Graph Model. 2020;96:107540. https://doi.org/10.1016/j.jmgm.2020.107540.
33. Kamaraj AB, Shaw V, Sundaram MM. Novel fabrication of un-coated super-hydrophobic aluminum via pulsed electrochemical surface modification. Procedia Manuf. 2015;1:892-903. https://doi.org/10.1016/j.promfg.2015.09.081.
34. Alberto M, Skuse C, Tamaddondar M, Gorgojo P. Immobilized graphene oxide-based membranes for improved pore wetting resistance in membrane distillation. Desalination. 2022;537:115898. https://doi.org/10.1016/j.desal.2022.115898.
35. Miyazaki CM, Mishra R, Kinahan DJ, Ferreira M, Ducrée J. Polyethylene imine/graphene oxide layer-by-layer surface functionalization for significantly improved limit of detection and binding kinetics of immunoassays on acrylate surfaces. Colloids Surf B Biointerfaces. 2017;158:167-74. https://doi.org/10.1016/j.colsurfb.2017.06.042.
36. Darmawan A, Zakiyah H, Muhtar H, Elma M. Graphene oxide/silicon dioxide (GO/SiO2) hybrid coating on zirconia ceramic for sustainable water desalination. Ceram Int. 2024;50(22 Suppl 22 Part B):47232-43. https://doi.org/10.1016/j.ceramint.2024.09.074.
37. Kobayashi M, Tashiro K, Tadokoro H. Molecular vibrations of three crystal forms of Poly(vinylidene fluoride). Macromolecules. 1975;8(2):158-71. https://doi.org/10.1021/ma60044a013.
38. Kabir E, Khatun M, Nasrin L, Raihan MJ, Rahman M. Pure β-phase formation in polyvinylidene fluoride (PVDF)-carbon nanotube composites. J Phys D Appl Phys. 2017;50(16):163002. https://doi.org/10.1088/1361-6463/aa5f85.
39. Zhu Y, Xie W, Zhang F, Xing T, Jin J. Superhydrophilic in-situ-cross-linked zwitterionic polyelectrolyte/pvdf-blend membrane for highly efficient oil/water emulsion separation. ACS Appl Mater Interfaces. 2017;9(11):9603-13. https://doi.org/10.1021/acsami.6b15682.
40. Chen E, Lu Y, Liu X, Song J, He G, Tiwari MK, et al. Table salt as a template to prepare reusable porous PVDF–MWCNT foam for separation of immiscible oils/organic solvents and corrosive aqueous solutions. Adv Funct Mater. 2017;27(41):1702926. https://doi.org/10.1002/adfm.201702926.
41. El-Bahnasy SS, Khalaf M, Ayad DM, Menazea AA. A green approach to improve antibacterial properties of PVC/PVDF film doped by silver nanoparticles via nanosecond laser ablation for wound healing application. Sci Rep. 2024;14(1):27926. https://doi.org/10.1038/s41598-024-78841-1.
42. Jiang J, Zhu L, Zhang H, Zhu B, Xu Y. Improved hydrodynamic permeability and antifouling properties of poly(vinylidene fluoride) membranes using polydopamine nanoparticles as additives. J Membr Sci. 2014;457:73-81. https://doi.org/10.1016/j.memsci.2014.01.043.
43. Shao L, Wang ZX, Zhang YL, Jiang ZX, Liu YY. A facile strategy to enhance PVDF ultrafiltration membrane performance via self-polymerized polydopamine followed by hydrolysis of ammonium fluotitanate. J Membr Sci. 2014;461:10-21. https://doi.org/10.1016/j.memsci.2014.03.006.
44. Li C, Liu W, Mao J, Hu L, Yun Y, Li B. Superhydrophobic PVDF membrane modified by dopamine self-polymerized nanoparticles for vacuum membrane distillation. Separ Purif Tech. 2023;304:122182. https://doi.org/10.1016/j.seppur.2022.122182.
45. Brusko V, Khannanov A, Rakhmatullin A, Dimiev AM. Unraveling the infrared spectrum of graphene oxide. Carbon. 2024;229:119507. https://doi.org/10.1016/j.carbon.2024.119507.
46. Ederer J, Ecorchard P, Slušná M, Tolasz J, Smržová D, Lupínková S, et al. A study of methylene blue dye interaction and adsorption by monolayer graphene oxide. Adsorpt Sci Technol. 2022;2022:7385541. https://doi.org/10.1155/2022/7385541.
47. Netzahual-Lopantzi A, García-Nieto E, Juárez-Santacruz L, Torres-Dorsal A, Gutiérrez-Fuentes R, García-Vidal UO, et al. Monitoring Congo red discoloration using thermal properties in photocatalytic processes: A new approach. Chem Eng Process. 2023;192:109506. https://doi.org/10.1016/j.cep.2023.109506.
48. Wang L, Wang A. Adsorption properties of Congo Red from aqueous solution onto surfactant-modified montmorillonite. J Hazard Mater. 2008;160(1):173-80. https://doi.org/10.1016/j.jhazmat.2008.02.104.
49. Debnath S, Maity A, Pillay K. Impact of process parameters on removal of Congo red by graphene oxide from aqueous solution. J Environ Chem Eng. 2014;2(1):260-72. https://doi.org/10.1016/j.jece.2013.12.018.
50. Kostjukova LO, Leontieva SV, Kostjukov VV. Vibronic absorption spectrum and electronic properties of methylene blue in aqueous solution: TD-DFT study. J Mol Liq. 2021;336:116369. https://doi.org/10.1016/j.molliq.2021.116369.
51. Azeez F, Al-Hetlani E, Arafa M, Abdelmonem Y, Nazeer AA, Amin MO, et al. The effect of surface charge on photocatalytic degradation of methylene blue dye using chargeable titania nanoparticles. Sci Rep. 2018;8(1):7104. https://doi.org/10.1038/s41598-018-25673-5.
52. Bensedira A, Haddaoui N, Doufnoune R, Meziane O, Labidi NS. Study of methylene blue dye elimination from water using polyaniline (PANI) and PANI/SiO_2 composite. Polym Polymer Compos. 2022;30:09673911221141747. https://doi.org/10.1177/09673911221141747.
53. Ball V. Impedance spectroscopy and zeta potential titration of dopa-melanin films produced by oxidation of dopamine. Colloids Surf A Physicochem Eng Asp. 2010;363(1-3):92-7. https://doi.org/10.1016/j.colsurfa.2010.04.020.

54. Oleg V, Ovchinnikov AV, Evtukhova TS, Kondratenko MS, Smirnov VY, Khokhlov OVE. Manifestation of intermolecular interactions in FTIR spectra of methylene blue molecules. Vib Spectrosc. 2016;86:181-9. https://doi.org/10.1016/j.vibspec.2016.06.016.
55. Ederer J, Ecorchard P, Slušná MŠ, Tolasz J, Smržová D, Lupínková S, et al. A study of methylene blue dye interaction and adsorption by monolayer graphene oxide. Adsorpt Sci Technol. 2022;2022:7385541. https://doi.org/10.1155/2022/7385541.
56. Mänttäri M, Pihlajamäki A, Nyström M. Effect of pH on hydrophilicity and charge and their effect on the filtration efficiency of NF membranes at different pH. J Membr Sci. 2006;280 (1-2):311-20. https://doi.org/10.1016/j.memsci.2006.01.034.
57. Mohammadikish M, Jorfi S. Growth of cobalt based-coordination polymer on the surface of filter paper for fast up-taking of Congo red by simple filtration. J Water Process Eng. 2022;47:102719. https://doi.org/10.1016/j.jwpe.2022.102719.
58. Nowik-Zajac A, Zawierucha I, Lagiewka J, Jaksender K, Witt K, Malina G, et al. Removal of methylene blue dye from aqueous solutions using polymer inclusion membrane containing Calix[4] pyrrole. Membranes. 2024;14(4):92. https://doi.org/10.3390/membranes14040092.
59. Bentahar S, Dbik A, El Khomri M, El Messaoudi N, Lacherai A. Adsorption of methylene blue, crystal violet and congo red from binary and ternary systems with natural clay: Kinetic, isotherm, and thermodynamic. J Environ Chem Eng. 2017;5(6):5921-32. https://doi.org/10.1016/j.jece.2017.11.003.
60. Yang L, Zhang Y, Liu X, Jiang X, Zhang Z, Zhang T, et al. The investigation of synergistic and competitive interaction between dye Congo red and methyl blue on magnetic $MnFe_2O_4$. Chem Eng J. 2014;246:88-96. https://doi.org/10.1016/j.cej.2014.02.044.
61. Spólnik P, Król M, Stopa B, Konieczny L, Piekarska B, Rybarska J, et al. Influence of the electric field on supramolecular structure and properties of amyloid-specific reagent Congo red. Eur Biophys J. 2011;40(10):1187-96. https://doi.org/10.1007/s00249-011-0750-z.
62. Florence N, Naorem H. Dimerization of methylene blue in aqueous and mixed aqueous organic solvent: A spectroscopic study. J Mol Liq. 2014;198:255-8. https://doi.org/10.1016/j.molliq.2014.06.030.
63. Lira-De León KI, García-Gutiérrez P, Serratos IN, Palomera-Cárdenas M, Figueroa-Corona MP, Campos-Peña V, et al. Molecular mechanism of tau aggregation induced by anionic and cationic dyes. J Alzheimers Dis. 2013;35(2):319-34. https://doi.org/10.3233/JAD-121765.
64. Schirg P, Widmer F. Characterisation of nanofiltration membranes for the separation of aqueous dye-salt solutions. Desalination. 1992;89(1):89-107. https://doi.org/10.1016/0011-9164(92)80154-2.
65. Xiao Q, Li W, Xie S, Wang L, Tang CY. Ultrafast complete dechlorination enabled by ferrous oxide/graphene oxide catalytic membranes via nanoconfinement advanced reduction. Nat Commun. 2024;15(1):9607. https://doi.org/10.1038/s41467-024-54055-x.
66. Chen X, Boffa V, Gaggero E, Meng F, Navone R, Sun D, et al. Metal-organic framework-intercalated graphene oxide nanofiltration membranes for enhanced treatment of wastewater effluents. Chem Eng J. 2024;486:150207. https://doi.org/10.1016/j.cej.2024.150207.
67. Sheikh S, Rahman M, Rahman S, Yildirim K, Maniruzzaman M. Fabrication of nano composite membrane filter from graphene oxide (GO) and banana rachis cellulose nano crystal (CNC) for industrial effluent treatment. J Ind Eng Chem. 2023;128: 196-208. https://doi.org/10.1016/j.jiec.2023.07.048.
68. Dey TK, Jamal M, Uddin E. Fabrication and performance analysis of graphene oxide-based composite membrane to separate microplastics from synthetic wastewater. J Water Process Eng. 2023;52:103554. https://doi.org/10.1016/j.jwpe.2023.103554.
69. Januário EFD, Vidovix TB, Calsavara MA, Bergamasco R, Vieira AMS. Membrane surface functionalization by the deposition of polyvinyl alcohol and graphene oxide for dyes removal and treatment of a simulated wastewater. Chem Eng Process. 2022;170:108725. https://doi.org/10.1016/j.cep.2021.108725.
70. Ahmad H, Zahid M, Rehan ZA, Rashid A, Akram S, Aljohani MMH, et al. Preparation of polyvinylidene fluoride nano-filtration membranes modified with functionalized graphene oxide for textile dye removal. Membranes. 2022;12(2):224. https://doi.org/10.3390/membranes12020224.
71. Subtil EL, Almeria Ragio R, Lemos HG, Scaratti G, García J, Le-Clech P. Direct membrane filtration (DMF) of municipal wastewater by mixed matrix membranes (MMMs) filled with graphene oxide (GO): towards a circular sanitation model. Chem Eng J. 2022;441:136004. https://doi.org/10.1016/j.cej.2022.136004.
72. Ma H, Wang G, Xu Z, Dong X, Zhang X. Confining peroxymonosulfate activation in carbon nanotube intercalated nitrogen doped reduced graphene oxide membrane for enhanced water treatment: the role of nanoconfinement effect. J Colloid Interface Sci. 2022;608:2740-51. https://doi.org/10.1016/j.jcis.2021.11.007.
73. Wang S, Liang S, Chen L, Fang H. Realizing ultrahigh nanofiltration performance based on small flake reduced graphene oxide membranes. Desalination. 2022;528:115601. https://doi.org/10.1016/j.desal.2022.115601.